Cryogenic Fluorescence Spectroscopy of Ionic Fluorones in Gaseous and Condensed Phases: New Light on their Intrinsic Photophysics

Eleanor K. Ashworth,[†,§] Jeppe Langeland,[‡,§] Mark H. Stockett,[¶] Thomas Toft Lindkvist,[‡] Christina Kjær,[‡] James N. Bull,[*,†] and Steen Brøndsted Nielsen[*,‡]

†*School of Chemistry, University of East Anglia, Norwich NR4 7TJ, United Kingdom*

‡*Department of Physics and Astronomy, Aarhus University, Aarhus 8000, Denmark*

¶*Department of Physics, Stockholm University, SE-10691 Stockholm, Sweden*

§*These authors contributed equally.*

E-mail: james.bull@uea.ac.uk; sbn@phys.au.dk

Abstract

Fluorescence spectroscopy of gas-phase ions generated through electrospray ionization is an emerging technique able to probe intrinsic molecular photophysics directly without perturbations from solvent interactions. While there is ample scope for the ongoing development of gas-phase fluorescence techniques, the recent expansion into low temperature operating conditions accesses a wealth of data on intrinsic fluorophore photophysics, offering enhanced spectral resolution compared with room temperature measurements, without matrix effects hindering the excited state dynamics. This perspective reviews current progress on understanding the photophysics of anionic fluorone dyes, which exhibit an unusually large Stokes shift in the gas phase, and discusses how comparison of gas- and condensed-phase fluorescence spectra can fingerprint structural

dynamics. The capacity for temperature-dependent measurements of both fluorescence emission and excitation spectra helps establish the foundation for the use of fluorone dyes as fluorescent tags in macromolecular structure determination. We suggest ideas for technique development.

Fluorescence spectroscopy

Fluorescence spectroscopy, whether in the infrared, visible, or ultraviolet, is an essential analytical technique in a chemist's toolkit.[1] Over the last few decades there has been an exponential increase in the adaptation and use of fluorescence techniques in applications including non-destructive chemical fingerprinting and structure determination, trace analyte and single-molecule detection, medicine, forensics and security, and biomolecule analysis.[2–4] The discovery of fluorescent proteins and the development of strategies for their incorporation into biotechnological applications has revolutionized modern microscopy, bioimaging, and the visualization of cellular processes.[5,6]

There are two flavors of fluorescence spectroscopy: (i) fluorescence emission spectroscopy (Figure 1a), which involves recording the emission spectrum at a given pump excitation wavelength, and (ii) fluorescence excitation spectroscopy (Figure 1b), which involves recording fluorescence yield at a given wavelength, or range of wavelengths, as a function of the pump excitation wavelength. In the instance when there is no wavelength-dependence to the fluorescence quantum yield, for example through competitive internal conversion pathways, the fluorescence excitation spectrum should parallel the absorption spectrum. Information embodied in the excitation and emission fluorescence spectra, fluorescence quantum yield, and Stokes shift (difference between maxima in absorption and fluorescence emission spectra) can inform on fluorophore concentration, chemical environment, and excited-state dynamical processes, such as nuclear rearrangements and energy-transfer mechanisms.

Gas-phase fluorescence

Despite fluorescence spectroscopy techniques being commonplace in industrial and academic settings, adaptation of fluorescence spectroscopy to gas-phase molecules has been sparse because the techniques are in their infancy.[7] Although there are many examples of gas-phase fluorescence from either small molecules (e.g., diatomics) with long-lived excited states[8]

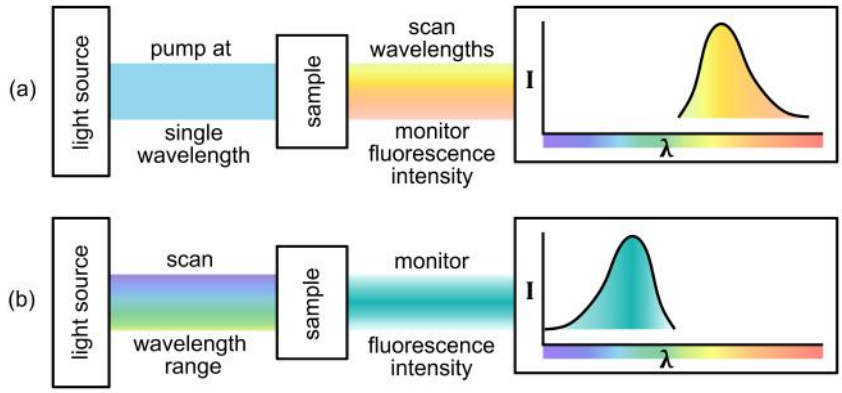

Figure 1: Fluorescence spectroscopy: (a) fluorescence emission spectroscopy, where the sample is excited at a given wavelength and the dispersed fluorescence spectrum is measured, (b) fluorescence excitation spectroscopy, where for each wavelength across a given range the fluorescence yield at a given wavelength is monitored.

or neutral molecules produced in molecular beam sources,[9] the generalization of gas-phase fluorescence to charged molecules produced from 'universal' ionization sources, such as electrospray ionization (ESI) or matrix-assisted laser desorption/ionization (MALDI), is limited. Some of the key advantages of studying fluorescence in the gas phase include: (i) the absence of condensed phase (solvent) environment, allowing both the intrinsic fluorescence properties of a fluorophore or molecular complex and the impact of solvation to be characterized, (ii) the straight-forward comparison of gas-phase studies with high-level quantum chemical calculations, and (iii) the ability to mass select the target ions, avoiding contaminations in non-pure samples – this may be particularly important for biomolecules that are difficult to purify.

Efforts to develop gas-phase fluorescence experiments coupled with ESI or MALDI sources over the last two decades have been summarized in Ref. 7. These instruments are based on 3D Paul,[10–17] Penning,[18,19] or LQT (linear quadrupole trap)[20,21] ion traps that accumulate and localize the ions into an irradiation volume. While each type of trap has advantages,[22] 3D Paul traps are simple and approximate a point-like trapping volume, making them easily adapted for fluorescence experiments. The majority of gas-phase fluorescence studies on ions generated through ESI have considered organic dyes, particularly rhodamines[10,14–16,23–28] and

other xanthene-based species[29–34] at $T = 300\,\mathrm{K}$ due to their desirable benchmarking characteristics. These investigations often provide a comparison to spectral properties in solution and contribute toward establishing a foundation from which tailored fluorophores can be developed. Most of these gas-phase studies have considered fluorescence emission spectra, with only a handful attempting to record fluorescence excitation spectra.[15,23,24,27,34] More sophisticated applications of gas-phase fluorescence spectroscopy have considered conformational studies of larger biomolecules, such as peptides, oligonucleotides, and proteins,[12,28,35,36] by exploiting Förster (fluorescence) resonance energy transfer (FRET) between through-space coupled fluorophores.[37]

The above-mentioned studies were performed almost exclusively at room-temperature; there are only a few reports of gas-phase fluorescence instruments incorporating cryogenic cooling of the ions (e.g., $T < 120\,\mathrm{K}$) through cooling of the ion trap and buffer gas with liquid nitrogen or attachment of the ion trap to a helium refrigerator.[13,17,21] The principal advantages of cryogenic cooling of the ions are (i) to increase spectral resolution, through the removal of hot bands, allowing for enhanced fingerprinting[17,38] (e.g., for FRET), and (ii) because decreasing temperature generally increases fluorescence quantum yield.

Fluorescence as an action spectroscopy

One of the main motivations for the development of gas-phase fluorescence spectroscopy instruments, particularly those offering fluorescence excitation spectra, is the capacity to be used for action spectroscopy. Specifically, while absorption spectra for ions in solution are easily recorded by monitoring the attenuation of light passed through a sample containing the target analyte at micromolar to millimolar concentration (10^{11}–10^{14} molecules/mm^3), the number of ions in a gas-phase experiment is many orders of magnitude lower (e.g., 10^3–10^6 molecules/mm^3). A direct absorption measurement in the gas-phase requires determining a minuscule change in light intensity. Although such measurements might be achievable using cavity ring-down strategies,[39,40] most gas-phase spectroscopy experiments

rely on measuring the appearance of a new, background-free signal generated as an 'action' resulting from the absorption of light.[41,42] Non-radiative 'actions' include dissociation, electron detachment, and isomerization.[43–45] There are many clear examples of action spectra recorded using these strategies that almost certainly parallel the underlying absorption spectrum; however, experimental conditions, including measurement time,[46,47] collision energy quenching,[48] non-uniform detection efficiency of ion fragments,[49] and competitive excited state dynamical processes, can skew the correspondence. A key benefit of using fluorescence as the 'action' in action spectroscopy is that the low-lying electronic absorption bands, e.g., $S_1 \leftarrow S_0$, are probed non-destructively, following the absorption of a single photon. In contrast, photodissociation (i.e., fragmentation) and photodetachment (i.e., electron ejection) action spectroscopies of ions with absorption bands in the visible or near-IR often rely on the absorption of two or more photons to exceed dissociation or electron detachment thresholds (3–4 eV).[43,44] This multi-photon absorption may skew the spectra toward the blue. For example, the absorption of two photons at 400 nm (blue) imparts 6.2 eV of internal energy while two 550 nm (green) photons imparts 4.5 eV, potentially leading to distinct fragmentation rates and patterns within the temporal acquisition window of the experiment (i.e., the kinetic shift in mass spectrometry).

Fluorone dyes

Fluorescein and derivatized fluorones (e.g., see Figure 2) are amongst the most important fluorescent dyes and are a cornerstone in fluorescence spectroscopy. They are widely used as fluorescent probes in bioimaging and technological applications due to their large absorption cross-section for visible light and high fluorescence quantum yield, e.g., $\phi_f > 0.9$ for many fluorones in common hydrogen-bonding solvents[50,51] and ≈0.5–0.7 in non-hydrogen-bonding solvents.[52] The fluorescence quantum yield of anionic fluorone dyes is high because access to the conical intersection(s) (CIs) associated with $S_1 \rightarrow S_0$ internal conversion is a barrier

controlled process, requiring simultaneous torsion of the carboxyphenyl moiety and flip-flop motion of the xanthene moiety.[53] The latter motion is hindered by reducing temperature and the presence of hydrogen-bonding networks in the condensed phase. Fluorescein and derivatives present a fascinating case to benchmark gas-phase experiments and to compare gas- and condensed-phase measurements at cryogenic temperatures (e.g., $T \approx 77$–$100\,\mathrm{K}$) because they are known to undergo excited state torsional motions that embody fingerprints in the Stokes shift.[32,54,55] Also, they offer a versatile molecular platform for developing fluorescent probes due to the synthetic capacity to modify groups on both the xanthene and carboxyphenyl moieties.[56,57] This capacity has seen fluorones as the basis for numerous design strategies of fluorescence probes for bioimaging and as 'on/off' sensors.[58–62]

Figure 2: Structures of fluorescein (FL), eosin Y (EY), and ethyl eosin (EE). As the gas-phase anion, deprotonation is on the xanthene moiety. The red hydrogen in FL was that proposed in Ref. 63 to convert FL-I to FL-II in a photoinduced proton transfer reaction.

The intriguing case of gas-phase fluorescein

The first gas-phase fluorescence study on fluorescein was performed by Jockusch and co-workers,[29] employing a modified commercial quadrupole ion trap mass spectrometer. They demonstrated that, although the dianion is the most fluorescent form in solution, it does not fluoresce in the gas-phase due to a short excited state lifetime to electron loss.[64] On the other hand, gas-phase fluorescein monoanions and two halogenated derivatives exhibited weak fluorescence signal with the halogenated derivatives having higher fluorescence quantum yields (consistent with their solution properties). Time-correlated single photon counting experiments gave gas-phase lifetimes of $\approx$5 ns.[30] Significantly, it was noted that the

fluorescence emission spectra were broader than for other xanthene-based dyes in the gas phase (e.g., rhodamine cations), potentially attributed to substantial nuclear relaxation on the excited state. Analysis of the Stokes shift with the aid of quantum chemical calculations and comparison with solution data concluded that deprotonation on the xanthene ring occurs in the gas phase (FL-I), corresponding to a different deprotomer than that residing in solution (FL-II). The assignment of deprotonation site was confirmed both through infrared multiphoton dissociation (IRMPD) studies[65] and through a recent ion mobility mass spectrometry study on rose bengal anions.[32]

In further work, Kjær *et al.*[63] used a homebuilt cylindrical ion trap mass spectrometer named LUNA (LUminescence iNstrument in Aarhus)[14] to measure the fluorescence from fluorescein and resorufin monoanions. The resorufin anion has the same xanthene core structure as fluorescein, except with the central carbon connecting the two benzene rings is replaced by nitrogen and without pendant carboxyphenyl group. They proposed the large Stokes shift ($\approx$2000 cm^{-1}) experienced by FL-I originates from a photo-induced proton transfer from the pendant carboxyphenyl group to an oxygen on the xanthene moiety, producing FL-II ($\approx$0.2 eV higher in energy than FL-I).[63] The assignment was consistent with earlier work on intramolecular proton transfer in ground-state fluorescein monoanions investigated in an ion storage-ring.[66] Furthermore, in support of the proton-transfer assignment, resorufin anions displayed narrow action spectra and a very small Stokes shift of $\approx$250 cm^{-1}. Subsequent studies on fluorescein methyl ester monoanions (no acidic proton) discarded the proton transfer explanation because the fluorescence spectrum was still broad with a band center (605 nm) shifted further to the red than that for fluorescein (590 nm).[31] In the same work, another fluorescein variant was studied where the carboxylic acid group was replaced by a bulky tertiary amide functionality, giving rise to a much smaller Stokes shift due to a closer similarity between the excited-state and ground-state structures. The excited state nuclear relaxation dynamics able to explain these spectra follows the model proposed by Verlet and co-workers,[54] developed from time-resolved photodetachment spectroscopy, where the

carboxyphenyl group rotates relative to the xanthene after photoexcitation of FL-I. This rotation results in an overlap between the π-orbitals of the xanthene and the carboxyphenyl moieties, enabling a partial electron transfer from the former to the latter.

From a theoretical perspective, the internal conversion dynamics of fluorones have been revised by Zhou *et al.*,[53] determining that a flip-flop motion of the xanthene moiety on the S_1 potential energy surface is needed in concert with rotation of the carboxyphenyl group. This motion results in a puckered geometry of the xanthene unit, leading to both a reduced fluorescence quantum yield and a large Stokes shift. For fluorescein monoanions, a CI between the S_1 and S_0 potential energy surfaces was predicted to lie $\approx$0.3 eV above the S_1 equilibrium geometry. Consequently, a significant amount of the internal energy needs to accumulate in the correct coordinates to reach the CI, ultimately leading to a long excited state lifetime ($\approx$5 ns).

Influence of temperature and the environment

The impact of temperature and environment on the fluorescence properties of anionic fluorones is illustrated through measurements on fluorescein (FL), eosin Y (EY), and ethyl eosin (EE), which are shown in Figure 2. Fluorescence emission and excitation spectra for the three anions in the gas and condensed phases are shown in Figure 3a-f, with the key spectral properties tabulated in Table 1.

The data presented in Figure 3 considers ion trap experiments utilizing a liquid nitrogen ($T \approx 77$ K) cooled ion trap; however, collisions and dissipation from the trap mean that the trapped ions will never reach $T \approx 77$ K, rather their temperature is estimated at $T \approx 100$ K. The condensed-phase experiments were performed at $T \approx 77$ K by immersing an EPR tube containing the sample in a liquid nitrogen bath. Despite this difference in temperature, we do not expect the gas or condensed phase spectroscopy and dynamics to vary significantly between the two temperatures. We also note that the freezing point of ethanol used as

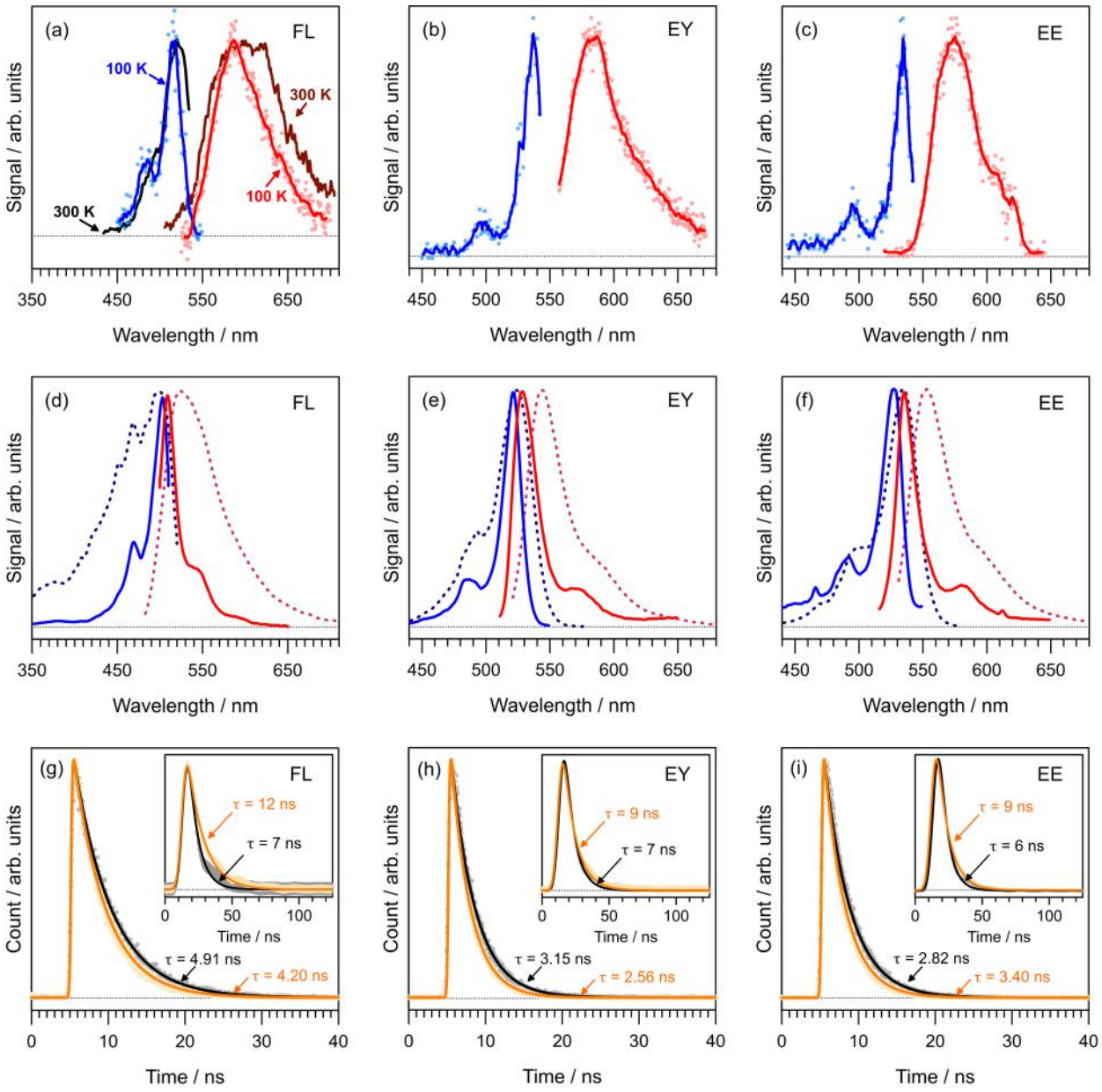

Figure 3: Fluorescence spectroscopy of FL, EY, and EE: (a)–(c) Gas-phase excitation (blue for $T \approx 100\,\mathrm{K}$, black for $T = 300\,\mathrm{K}$) and emission (red for $T \approx 100\,\mathrm{K}$, brown for $T = 300\,\mathrm{K}$ – pumped at 514 nm for FL and 533 nm for EY and EE) spectra. Solid lines are five-point moving averages. The red edges of the fluorescence excitation spectra for EY and EE are not available because of the long-pass filters used to avoid excitation light. (d)–(f) Condensed phase excitation (blue) and emission (red) spectra at $T \approx 77\,\mathrm{K}$ (solid lines) and $T = 300\,\mathrm{K}$ (dashed), pumped at 490 nm ($T \approx 77\,\mathrm{K}$) and 470 nm ($T = 300\,\mathrm{K}$) for FL, 500 nm ($T \approx 77\,\mathrm{K}$) and 510 nm ($T = 300\,\mathrm{K}$) for EY, and 500 nm ($T \approx 77\,\mathrm{K}$) and 520 nm ($T = 300\,\mathrm{K}$) for EE. (g)–(i) Condensed phase (gas phase in inset) fluorescence lifetimes at $T \approx 77\,\mathrm{K}$ (orange, $T \approx 100\,\mathrm{K}$ for inset) and $T = 300\,\mathrm{K}$ (black). Uncertainties in the fitted lifetimes are ± 0.02 ns and ± 1 ns for condensed- and gas-phase data, respectively. Condensed phase measurements were performed in ethanol. Horizontal dotted lines in each panel indicates the zero signal level.

the solvent in the condensed phase measurements, is much higher (at $T = 160\,\mathrm{K}$), so the viscosity will not change over the $T = 77$–$100\,\mathrm{K}$ range. On a related note, the issue of 'ion temperature' in a gas-phase experiment utilizing an ion trap is often difficult to determine precisely. The trapped ions are constrained by radio frequency (RF) fields, i.e., the ions experience non-zero forces and constant collisions with the helium buffer gas atoms. 'Room temperature' measurements (i.e., no cryo-cooling), however, are likely close to $T = 300\,\mathrm{K}$ because, as shown in the the investigations by Gronert[67] using thermometer reactions, the effective temperature of a quadrupole ion trap is $T = 310 \pm 20\,\mathrm{K}$. To estimate an effective temperature of the cryogenic cold ions in the LUNA2 ion trap, we would need to compare temperature-dependent simulations with fluorescence excitation spectra of an ion with well-resolved hot bands.

Returning to Figure 3, for FL at $T = 300\,\mathrm{K}$, the gas-phase fluorescence excitation spectrum is substantially narrower than the fluorescence emission spectrum, with the pair giving a large Stokes shift of $\approx 2000\,\mathrm{cm}^{-1}$. On the other hand, cooling FL to $T \approx 100\,\mathrm{K}$ slightly sharpens both spectra, and results in a small increase in the Stokes shift to $\approx 2400\,\mathrm{cm}^{-1}$. These gas-phase spectra contrast with the condensed-phase (ethanol) data, where, at $T = 300\,\mathrm{K}$, the fluorescence excitation and emission spectra are both broad and exhibit a small Stokes shift of $\approx 500\,\mathrm{cm}^{-1}$. Cooling of the solution to $T \approx 77\,\mathrm{K}$ significantly sharpens the fluorescence excitation and emission spectra but reduces the Stokes shift to a mere $\approx 200\,\mathrm{cm}^{-1}$. Similar trends are seen for the gas-phase and condensed-phase spectra for EY and EE. These marked differences in spectral breadth and Stokes shift are characteristic to the fluorones and are uncommon in other dye molecules.

Jablonski diagram

To understand the fluorone spectra presented in Figure 3, we consider the Jablonski diagram shown in Figure 4. In the condensed phase (Figure 4a), vibrational energy relaxation to the environment can occur, and is usually complete after a few to tens of picoseconds.[68] In Fig-

Table 1: Fluorescence excitation (ex) and emission (em) spectra wavelength maxima, in nm, for the target anions in the gas phase at $T \approx 100\,\mathrm{K}$ ($T = 300\,\mathrm{K}$ in parentheses) and condensed phase at $T \approx 77\,\mathrm{K}$ ($T = 300\,\mathrm{K}$ in parentheses). Theory values were computed at the DLPNO-STEOM-CCSD/def2-SVPD level. Stokes shift, $\Delta\nu$, is in units of cm^{-1}.

	Gas phase			Theory		
Species	λ(ex)[a]	λ(em)[a]	$\Delta\nu$	λ(ex)	λ(em)	$\Delta\nu$
FL	517 (525)[b]	589 (590)[b]	2364 (2098)	530[c]	598[d]	2145
EY	537	582	1440	550	582[d]	1003
EE	534	576	1365	563	595	955
	Condensed phase					
Species	λ(ex)[e]	λ(em)[e]	$\Delta\nu$			
FL	503 (498)	509 (526)	234 (1069)			
EY	521 (524)	528 (544)	254 (702)			
EE	526 (535)	535 (552)	320 (576)			

[a] $\pm 2\,\mathrm{nm}$ uncertainty; [b] $\pm 5\,\mathrm{nm}$ uncertainty (Ref. 31); [c] 404 nm for the carboxylate deprotomer; [d] calculated value assumes the LC-ωHPBE/def2-SVPD relaxation energy on the S_1 state; [e] $\pm 1\,\mathrm{nm}$ uncertainty.

ure 4a, we term this solvent dissipation (SD). Since solvent dissipation is rapid compared with typical fluorescence lifetimes (ca. nanoseconds at $T = 300\,\mathrm{K}$), and due to the Franck-Condon principle, there is usually a 'mirror image' relationship between absorption (fluorescence excitation) and fluorescence emission spectra.[69] When temperature is decreased, the spectra sharpen and the Stokes shift decreases (the emission spectrum becomes blue shifted) because there is an increase in viscosity or formation of a glassy matrix and, consequently, hindrance of excited-state motions of both the fluorophore and the solvent cage that contribute to the Stokes shift.

The gas-phase situation depicted in Figure 4b has no solvent dissipation process. Specifically, the ions in an ion trap experience vibrational energy quenching collisions only every few nanoseconds such that excess vibrational energy in the molecule is not quenched over the excited state lifetime, leading to broadening of the fluorescence emission spectrum – this is usually more evident at low temperatures and when there is substantial nuclear rearrangement (as is the case for the fluorones). In the general case, a slight decrease in the gas-phase Stokes shift accompanies decreasing temperature;[33] however, the fluorones present an interesting exception because 'floppy' excited state nuclear motions are never hindered

(discussed further below) – it is this property that makes them suited for structural fingerprinting of gas-phase versus condensed-phase complexes as a function of temperature, e.g., when incorporated into macromolecular systems or FRET applications.

Returning to the cryogenic fluorescence excitation and emission spectra shown in Figure 3, the gas-phase fluorescence emission spectra for each of the fluorone anions are examples of the case illustrated in Figure 4c (middle) where the excess vibrational energy following nuclear relaxation is not quenched and leads to a broadened emission spectrum (Figure 4b). On the other hand, the $T \approx 77\,\mathrm{K}$ condensed-phase spectra resemble the situation illustrated in Figure 4c (lower) due to the solvent dissipation process.

Torsional and structural dynamics

The excited-state nuclear relaxation dynamics of fluorone dyes leading to the large gas-phase Stokes shift involves a rapid twist of the carboxyphenyl ring relative to the xanthene moiety (Figure 5) combined with a slight puckering of the xanthene moiety.[32,53] Calculated dihedral angles, ϕ, for the S_0 and S_1 states of FL, EY, and EE are summarized in Table 2. For example, for EY, $\phi = 92°$ in the S_0 equilibrium geometry, which becomes $\phi = 59°$ on the S_1 state. The Stokes shift in the condensed phase at $T \approx 77\,\mathrm{K}$ is an order of magnitude smaller because the torsional nuclear motion on the S_1 state is hindered (frozen) in the glassy matrix.

Thus, while cooling significantly sharpens gas- or condensed-phase excitation spectra, there is only a minor sharpening of gas-phase fluorescence emission spectra because the vibrational temperatures exceed the nuclear relaxation energy (calculated at $\approx$0.2 eV for FL and $\approx$0.1 eV for both EY and EE), meaning that the gas-phase excited state ions may fluoresce from a range of non-equilibrium geometries and have significant hot bands. Furthermore, the fluorescence emission spectrum will be broadened further when using an excitation wavelength to the blue of the 0-0 transition.

Concurrent with the substantial variation in the Stokes shift between the gas and condensed phases, due to the occurrence or inhibition of excited state nuclear dynamics, there

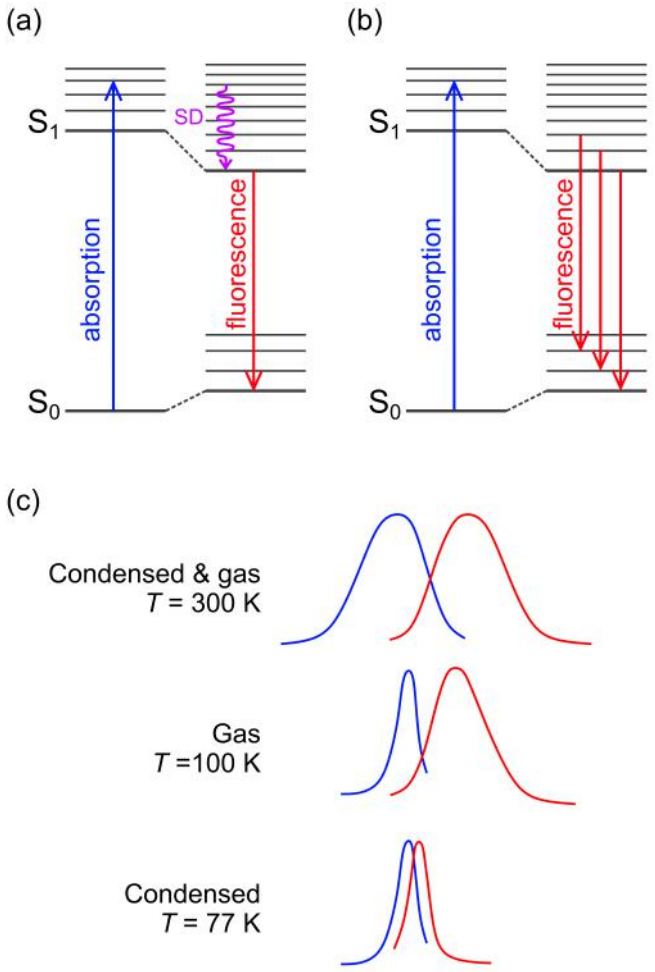

Figure 4: (a)–(b) Jablonski diagram for fluorescence in: (a) condensed phase and (b) gas phase. SD indicates intermolecular redistribution of energy to the solvent (solvent dissipation), a process which is absent in gas-phase experiments because fluorescence occurs more rapidly than collisional energy quenching. The diagrams consider nuclear relaxation on the S_1 state, e.g., through torsional motion of the ring systems for fluorones.[32,54] (c) Representation of fluorescence excitation (blue) and emission (red) spectra of a given species in gas and condensed phases with temperature. Note: the gas-phase fluorones present an unusual case in which the Stokes shift increases with decreasing temperature due to dynamics on the excited state.

are also changes in transition probability, affecting the fluorescence quantum yield (and excited state lifetimes). Calculated electronic transition oscillator strengths, f, for the fluorone anions at the S_0 and S_1 equilibrium geometries are given in Table 2. These values show a reduced fluorescence oscillator strength at the S_1 geometry due to decreased overlap between the π-orbitals on the ring systems.

The occurrence of torsional dynamics is important in a broad range of other systems, including chromophores in photoactive proteins,[70,71] light-driven molecular machines,[72] and photoswitch molecules used in technology,[73] such as photopharmacology. These dynamics are often difficult to discern directly in a single experiment. The strategy for understanding the torsional dynamics in the fluorones in this work, combining data from gas-phase and condensed-phase spectroscopies, may be generalized to these other chromophore systems.

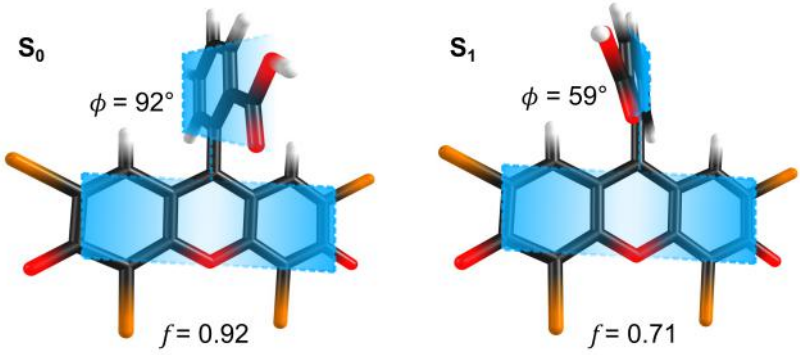

Figure 5: Illustrations of the S_0 and S_1 geometries for EY. Parameter ϕ is the xanthene-carboxyphenyl dihedral angle and f is the vertical oscillator strength. In the S_1 geometry, there is a slight puckering of the xanthene moiety and torsion of the carboxylate/ester group. Calculated values for the other anions are given in Table 2.

Deprotomers

The spectral interpretations consider monoanions deprotonated on the xanthene moiety. However, fluorescein-based dyes with free carboxylic acid functional groups on the carboxyphenyl moiety may exist as carboxylate deprotomers and a cyclized lactone tautomer (e.g., Figure 6).[74] For rose bengal monoanions, we used ion mobility spectrometry to demon-

strate that ESI from methanol generates only the xanthene-deprotonated isomer. Furthermore, calculations of vertical excitation wavelengths for the carboxylate or lactone forms indicate the $S_1 \leftarrow S_0$ band is in the near-UV, which is outside of the visible optical window. We note that the spectra for EY and EE are similar, suggesting similar deprotonation, and also the correspondence between the gas-phase ($T \approx 100\,\mathrm{K}$) and condensed-phase ($T \approx 77\,\mathrm{K}$) excitation spectra, indicating that the same deprotomers are fluorescing in both phases. In summary, there are no spectral contributions from the carboxylate deprotomers or lactone forms of the anions generated in the ESI process.

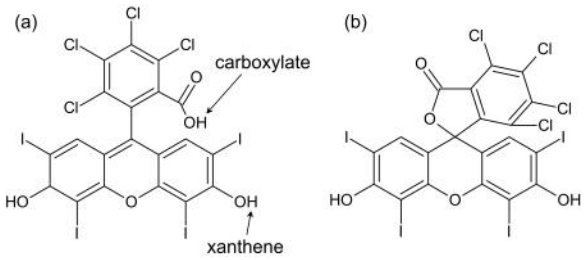

Figure 6: Deprotomers of rose bengal: (a) deprotonation on the carboxylic acid and xanthene groups gives rise to the carboxylate and xanthene deprotomers, respectively. The xanthene deprotomer is the most stable gas-phase form. (b) lactone deprotomer of rose bengal, where deprotonation would be on the xanthene moiety. FL and EY may exhibit similar deprotomers. Conversion of the carboxylate group to an ester blocks the carboxylate deprotomer.

Table 2: Dihedral angles, ϕ, and oscillator strengths, f, for the fluorone anions, calculated at the LC-ωHPBE/def2-SVPD level.

	ϕ			f		
	FL	EY	EE	FL	EY	EE
S_0	107°	92°	70°	0.80	0.92	0.88
S_1	130°	59°	57°	0.40	0.71	0.79

Fluorescence lifetimes

Fluorescence lifetimes for the three fluorone anions are shown in Figure 3g–i [$T \approx 77$ or 100 K (orange) and $T = 300\,\mathrm{K}$ (black)]. In the gas phase, the $T \approx 100\,\mathrm{K}$ lifetimes are several nanoseconds longer than for the $T = 300\,\mathrm{K}$ ions, due to suppression of the internal conversion

pathway. Specifically, the rate constant for loss of the excited state is $k = k_f + k_{IC}$, where k_f is the fluorescence rate constant and k_{IC} is the internal conversion rate constant. Theoretical calculations by Zhou *et al.*[53] have shown that internal conversion in FL involves a barrier of $\approx$0.43 eV, meaning that k_{IC} decreases (and k_f increases) with decreasing temperature. As an approximate quantification, in terms of initial vibrational energies calculated from harmonic partition functions, the average thermal energy of the ions at $T = 300$ K is 0.51 eV (FL), 0.68 eV (EY), and 0.76 eV (EE), and are 0.08 eV (FL), 0.11 eV (EY), and 0.12 eV (EE) at $T \approx 100$ K. Thus, while the barrier can be surmounted at $T = 300$ K following excitation at the band origin, higher photon energies are needed at $T \approx 100$ K.

The condensed-phase fluorescence lifetimes present an unusual situation because the fitted lifetimes at $T = 300$ K are slightly longer than those at $T \approx 77$ K. This peculiarity can be understood in terms of the torsional dynamics and changes in oscillator strength described above. Specifically, at $T = 300$ K, torsional motion on the excited state occurs and leads to a geometry with a lower oscillator strength (and, therefore, lower k_f). On the other hand, at $T \approx 77$ K the molecules are fixed in the Franck-Condon geometry, which has a higher oscillator strength for fluorescence (and, consequently, higher k_f). Because k_{IC} should increase and k_F decrease with increasing temperature, the condensed-phase measurements are in a regime where the decrease in k_f is larger than the increase in k_{IC}.

The occurrence of these torsional dynamics could be useful for informing on macromolecular conformations, for example, in protein structures,[36] through the incorporation of two fluorescing molecules, such as fluorone dyes, into the macromolecular system. Such tagging enables FRET studies, due to energy transfer between the fluorophores. FRET rates and efficiencies are determined by the inter-fluorophore separation which, in turn, reflect macromolecular structure/conformation.[12,28,35] Additionally, gas-phase fluorescence emission spectra of these tagged macromolecules recorded at $T \approx 100$ K may be more comparable to $T \approx 77$ K condensed-phase measurements (excluding the solvent effects) because the excess vibrational energy after nuclear rearrangement is distributed to the entire macromolecular

backbone.

Gas-phase brightness – Temperature dependence

A current challenge in gas-phase fluorescence spectroscopy is measurement of fluorescence quantum yields or even relative brightness. To provide a rough estimate of the relative brightness for FL at $T = 300\,\mathrm{K}$ and $T \approx 100\,\mathrm{K}$, we invoke the following assumptions: (i) the absorption cross-section of the gas-phase electronic transition is independent of temperature (i.e., areas under respective absorption curves are the same), (ii) the ion density in the trap is independent of temperature, and (iii) the overlap between the laser pulse and the ion cloud is independent of temperature. Based on these assumptions, the ratio between the brightness, γ, at the two temperatures is given by

$$\gamma = \frac{Y_{100\,\mathrm{K}}(516\,\mathrm{nm})}{Y_{300\,\mathrm{K}}(525\,\mathrm{nm})} \frac{\sigma_{300\,\mathrm{K}}(525\,\mathrm{nm})}{\sigma_{100\,\mathrm{K}}(516\,\mathrm{nm})} \frac{N(516\,\mathrm{nm})}{N(525\,\mathrm{nm})}$$

where Y represents the yield of emitted photons, σ the absorption cross section, and N the number of photons. Multiple yield brightness measurements with a photomultiplier tube were performed at the FL absorption band maximum at $T \approx 100\,\mathrm{K}$ (516 nm) and at $T = 300\,\mathrm{K}$ (525 nm) to give a relative brightness of $\gamma \approx 2$. This increase in brightness with decreasing temperature is consistent with the change in excited-state lifetimes.

Current challenges and directions

Experimental considerations

A general property of gas-phase fluorescence, particularly for bare fluorophores, is a lower fluorescence quantum yield compared with the same molecules in solution, due to the lack of vibrational energy quenching. While cooling of the ions generally increases the fluorescence quantum yield, it does not result in the same increase in fluorescence quantum yield as for

molecules in the condensed phase (the present fluorone anions are an exception in that fluorescence quantum yield in the condensed phase decreases with decreasing temperature). In addition to the capacity for low-temperature fluorescence spectra, there are three key properties to consider when designing gas-phase fluorescence instrumentation: (i) maximization of fluorescence photon detection, (ii) maximization of the number of irradiated ions, and (iii) addition of further mass spectrometry sectors for probing of photodegradation or for providing isomer selection.

Photon detection

Increasing the number of detected fluorescence photons in a gas-phase experiment is the obvious route for increasing measurement efficiency, decreasing detection limits, and decreasing spectral acquisition time. The most efficient gas-phase fluorescence instruments utilizing 3D Paul traps have replaced the solid trap electrodes with wires or mesh grids, allowing photons to escape from the trap, although typically only $\approx$10% of fluorescence light is captured. Further losses are associated with filtering optics used to remove scattered excitation light. As a specific example, the LUNA2 apparatus, used to acquire the fluorone data presented above, is estimated to detect fluorescence from ions with fluorescence quantum yield $>$0.001 (i.e., 0.1%) using a 3D Paul trap in which the exit electrode is a mesh grid. Still, the collection efficiency is estimated at $\approx$5% and acquisition of a typical emission fluorescence spectrum may take several to tens of minutes. LQTs offer the most open geometries for fluorescence photon detection but also have a more extended ion trapping volume, making efficient fluorescence accumulation difficult with classical optics, and are usually associated with more sophisticated instrument development (particularly cooling). Because modern detectors, such as intensified CCD cameras, claim exceptionally high detection efficiencies across the visible and near-IR, development efforts are best placed on optimizing photon collection efficiency rather than detector technology. One potential development might involve use of a large, tapered fiber-optic bundle or rod rather than light collection lenses, which

could be positioned closely around the ion trap and connect via a vacuum feedthrough to relevant filters and the detector.

One of the complications in gas-phase fluorescence spectroscopy experiments is competitive photodissociation (or photodetachment for anions with low electron binding energies) of the trapped ions, leading to their destruction.[32,36] In fact, the probability of photodissociation may be several orders of magnitude larger than that for fluorescence. For this reason, ideal gas-phase fluorescence experiments should refresh the trapped ions every laser shot. As an example, we recently investigated fluorescence from anionic rose bengal,[32] where the dianion $[\text{RB-2H}]^{2-}$ was non-fluorescent but readily photodetached to give the fluorescent radical monoanion $[\text{RB-2H}]^{\bullet-}$. However, the parent monoanion $[\text{RB-H}]^{-}$ is fluorescent, possesses a distinct Stokes shift, and is difficult to isolate from $[\text{RB-2H}]^{\bullet-}$ because of a similar m/z. It is conceivable, for a macromolecular structure containing one or more fluorophores, that photodissociation may produce fragments with distinct fluorescence properties, thereby complicating the spectra. It is desirable that an experiment can control the refresh rate of the trap relative to the number of laser shots, and have provision to probe any photofragmentation generated in the trap, for example through a subsequent mass spectrometry stage.

Acquisition rate

The rate of acquisition of a gas-phase fluorescence spectrum can be maximized by increasing the number of trapped ions that fluoresce and/or by increasing the repetition rate of the measurement. As outlined above, there have been several types of ion trap deployed in gas-phase fluorescence spectroscopy instruments, with most favouring the simple 3D Paul trap due to ease of interfacing with lasers.[75] However, such traps are easily saturated at hundreds of thousands to millions of ions and offer a limited mass-to-charge range ($\approx$4000).[22,76] Thus, an obvious alternative direction is to increase the experimental repetition rate. Because many tunable lasers (e.g., OPOs) utilize flash-lamp YAG pump lasers, their repetition rate is usually limited to 10 or 20 Hz. The availability of tunable wavelength picosecond OPOs

offer both faster repetition rates (e.g., 50–1000 Hz) and the possibility for time-resolved fluorescence measurements when coupled with a gated detector. Such an arrangement would allow for the investigation of excited state lifetime as a function of excitation wavelength. While the fluorescence lifetimes for molecules in the condensed phase usually have little to no dependence on the excitation wavelength, because excess internal vibrational energy is rapidly quenched, similar quenching does not occur in the gas phase. Wavelength-dependent studies of excited state lifetimes (particularly for cooled ions) should provide an avenue to explore features of the excited state potential energy surface, such as barriers to CIs leading to internal conversion.[53]

Additional sectors

An interesting direction for the development of gas-phase fluorescence spectroscopy involves coupling with ion mobility spectrometry, allowing for isomer or shape selectivity of the trapped ions and, thus, measurement of fluorescence excitation and emission spectra for single macromolecular conformations.[77,78] Briefly, ion mobility can select ions of a given shape based on their collision cross-section with an inert buffer gas (usually He or N_2).[79] The technique is widely available in commercial mass spectrometry for protein and macromolecular conformation analysis, and has seen incorporation into gas-phase spectroscopy experiments.[7] For small chromophore ions, ion mobility can readily separate ring open and closed isomers,[45,80] *E-Z* isomers,[48] protomers,[81] and tautomers,[82] allowing for characterization of the photophysical properties of each form. While the coupling of an ion mobility sector with gas-phase fluorescence has been demonstrated,[77] including for recording the fluorescence spectrum of the green fluorescent protein,[78] the strategy has not been extended to investigate isomers. In the context of FRET experiments, the isomer selectivity provided by ion mobility permits separation and selection of macromolecular conformations prior to fluorescence probing,[83] thereby allowing for more defined measurements, such as stages in a protein-folding or unfolding mechanism.[84,85] The FRET parameters could be combined

with modelling of ion mobility collision cross-section, providing a more rigorous structural characterisation.

A notable advantage of gas-phase fluorescence experiments, compared to solution-based measurements, is mass selectivity. Specifically, gas-phase fluorescence experiments incorporating mass spectrometry sectors allow for mass-to-charge selection of ions before injection into the trap and/or during the ion trap storage cycle. This mass selectivity is useful for removing contaminants, particularly for fluorescent biological samples for which purification is difficult. Furthermore, the mass selectivity allows for the possibility to probe hydrated systems (from small organic molecules to macromolecules), developing the connection between gas- and condensed-phase fluorescence properties and allowing the impact of a given solvent to be investigated in a systematic manner.[86,87] However, because solvent molecules are usually weakly bound (e.g., tens of $\mathrm{kJ\,mol^{-1}}$ for weakly interacting systems), cryogenic temperatures are crucial for avoiding solvent molecule evaporation. To date, we are unaware of any such gas-phase fluorescence studies, although we note efforts to study fluorescence from partially solvated ions in electrospray plumes.[88–91]

The examples presented in this perspective involved ions cooled to $T \approx 100\,\mathrm{K}$, achieved using a liquid nitrogen cooled ion trap. Cooling of ion traps and their contents to $T \approx 10$–$20\,\mathrm{K}$ is becoming increasing common in the gas-phase spectroscopy community using helium refrigerators,[75] and should lead to significantly higher resolution in fluorescence excitation spectra and, presumably, quantum yields. To date, there is only one example of the coupling of a helium refrigerator with a LQT as part of a fluorescence experiment,[21] but we expect adaptation of other gas-phase fluorescence instruments in the near future.

Final remarks

This perspective has considered the gas-phase fluorescence properties of anionic fluorone dyes, demonstrating how gas-phase and condensed-phase data can complement one another

to fingerprint excited state dynamics. In many regards, gas-phase fluorescence spectroscopy is still in the early stages of development, still requiring benchmark measurements. Anionic fluorone dyes provide a clear example of the relationships between low temperature gas- and condensed-phase fluorescence excitation and emission spectra, and serves to highlight the utility of gas-phase fluorescence excitation as the foundation for action spectroscopy. The present approach of comparing low-temperature gas- and condensed-phase fluorescence data with supporting computations may readily be extended to other dye or chromophore systems with similar excited state dynamics, including those undergoing photoisomerization, tautomerization, or ring-opening and closing reactions. Although this perspective has considered isolated dye molecules, low-temperature gas-phase fluorescence spectroscopy is also applicable to larger biological or macromolecular systems tagged with dye molecules. This enables low-temperature FRET-based measurements and also the characterization of dynamics, such as inter-fluorophore separation, that might be complicated in the condensed phase due to sample freezing.

Author contributions

Gas-phase fluorescence spectroscopy experiments at $T \approx 100$K were recorded as part of a research visit by EKA, MHS, and JNB to the laboratory of SBN. All authors contributed to the gas-phase experimental data collections, with additional measurements performed by JL. EKA performed all condensed-phase measurements and electronic structure calculations. The manuscript was drafted by EKA and JNB with contributions from all authors.

Acknowledgement

Funding was provided by the Swedish Foundation for International Cooperation in Research and Higher Education (STINT, grant number PT2017-7328 to M.H.S. and J.N.B.), an EPSRC New Investigator Award (EP/W018691 to J.N.B.). E.K.A. thanks the University of

East Anglia for doctoral studentship. S.B.N. acknowledges support from the NOVO Nordisk Foundation (grant number NNF20OC0064958) and Carlsbergfondet (grant number CF20-0097). Electronic structure calculations were carried out on the High Performance Computing Cluster supported by the Research and Specialist Computing Support service at the University of East Anglia.

Supporting Information Available

Experimental and theoretical methods. Absorption spectra for FL, EY, and EE in ethanol. Optimized geometries for the S_0 and S_1 electronic states of FL, EY, and EE.

Biographies

Eleanor Ashworth completed a MChem at the University of York and a MScR (Masters by Research) in chemistry at University of East Anglia (UEA). She is currently working towards a PhD at UEA, which involves developing a new gas-phase experiment combining ion mobility spectrometry, ion trapping, time-of-flight mass spectrometry, and velocity-map imaging.

Jeppe Langeland received his PhD in physics from Aarhus University in 2019, including a stay at the University of Melbourne. He has worked with climate science and greenhouse gases as postdoctoral researcher at Aalborg University and at Aarhus University since 2020 in the group of Steen Brøndsted Nielsen. His research interests are mainly focused on the development of new instrumentation for gas-phase fluorescence spectroscopy.

Mark Hugo Stockett earned his PhD in physics from the University of Wisconsin in 2011. He was a postdoctoral researcher at Stockholm University (SU) and Aarhus University and is now Docent in Physics at SU. His research uses action spectroscopy to probe the photophysics of molecular ions in the gas phase and their interaction at interfaces.

Thomas Toft Lindkvist received his BSc in physics from Aarhus University in 2022.

The focus of his thesis work was mass spectrometry and cryogenic ion fluorescence spectroscopy. He has been a summer student at CERN and is currently a graduate student at Aarhus University.

Christina Kjær received her PhD in physics from Aarhus University in 2019, including a stay at the University of Melbourne where she worked with ion mobility spectrocopy. She is a postdoctoral researcher at Aarhus University, since 2019 in the group of Steen Brøndsted Nielsen. Her research interests are mainly focused on the photophysics of ionic dyes and the development of new instrumentation for gas-phase fluorescence spectroscopy.

James Bull completed his undergraduate and PhD in chemistry at the University of Canterbury, New Zealand. Following a series of postdoctoral studies at Oxford University, Durham University, and the University of Melbourne, he started as a Lecturer in Ultrafast Chemical Physics at University of East Anglia. His research involves the application of gas-phase spectroscopies to probe fundamental photochemical dynamics.

Steen Brøndsted Nielsen received his PhD degree in physical chemistry from the University of Copenhagen in 2000, including a stay at Yale University. He was a postdoctoral researcher at Aarhus University (AU) and Princeton University. After positions as Assistant Professor and Associate Professor at AU, he was promoted to Full Professor in 2019. He has been Guest Professor at Université Parid-Sud 11, Université de Caen Basse Normandie, and Université Paris 13 and a JILA Visiting Fellow. His research interests are within mass spectroscopy with special focus on the effect of a microenvironment on the spectroscopic properties of (bio)molecular ions using home-built setups.

References

(1) Lakowicz, J. R. *Principles of Fluorescence Spectroscopy*; Springer, 2006.

(2) Valeur, B.; Brochon, J.-C. *New Trends in Fluorescence Spectroscopy Applications to Chemical and Life Sciences*; Springer, 2001.

(3) Gurtler, V. *Fluorescent Probes*; Elsevier Science & Technology, 2021.

(4) Jones, B. J. *Springer Handbook of Microscopy*; Springer International Publishing, 2019; pp 1507–1524.

(5) Lichtman, J. W.; Conchello, J.-A. Fluorescence Microscopy. *Nat. Meth.* **2005**, *2*, 910–919.

(6) Wilhelmsson, M.; Tor, Y. *Fluorescent Analogues of Biomolecular Building Blocks*; John Wiley & Sons Inc., 2016.

(7) Zettergren, H.; Domaracka, A.; Schlathölter, T.; Bolognesi, P.; Díaz-Tendero, S.; Łabuda, M.; Tosic, S.; Maclot, S.; Johnsson, P.; Steber, A. et al. Roadmap on Dynamics of Molecules and Clusters in the Gas Phase. *Eur. Phys. J. D* **2021**, *75*, 152.

(8) Kinsey, J. L. Laser-Induced Fluorescence. *Annu. Rev. Phys. Chem.* **1977**, *28*, 349–372.

(9) Nakajima, A. Fluorescence Emission in the Gas Phase of Several Aromatic Hydrocarbons. *Bull. Chem. Soc. Japan* **1972**, *45*, 1687–1695.

(10) Khoury, J. T.; Rodriguez-Cruz, S. E.; Parks, J. H. Pulsed Fluorescence Measurements of Trapped Molecular Ions With Zero Background Detection. *J. Am. Soc. Mass Spectrom.* **2002**, *13*, 696–708.

(11) Sassin, N. A.; Everhart, S. C.; Dangi, B. B.; Ervin, K. M.; Cline, J. I. Fluorescence and Photodissociation of Rhodamine 575 Cations in a Quadrupole Ion Trap. *J. Am. Soc. Mass Spectrom.* **2009**, *20*, 96–104.

(12) Talbot, F. O.; Rullo, A.; Yao, H.; Jockusch, R. A. Fluorescence Resonance Energy Transfer in Gaseous, Mass-Selected Polyproline Peptides. *J. Am. Chem. Soc.* **2010**, *132*, 16156–16164.

(13) Kordel, M.; Schooss, D.; Neiss, C.; Walter, L.; Kappes, M. M. Laser-Induced Fluorescence of Rhodamine 6G Cations in the Gas Phase: A Lower Bound to the Lifetime of the First Triplet State. *J. Phys. Chem. A* **2010**, *114*, 5509–5514.

(14) Stockett, M. H.; Houmøller, J.; Støchkel, K.; Svendsen, A.; Nielsen, S. B. A Cylindrical Quadrupole Ion Trap in Combination with an Electrospray Ion Source for Gas-Phase Luminescence and Absorption Spectroscopy. *Rev. Sci. Instrum.* **2016**, *87*, 053103.

(15) Honma, K. Laser-Induced- and Dispersed-Fluorescence Studies of Rhodamine 590 and 640 Ions Formed by Electrospray Ionization: Observation of Fluorescence From Highly-Excited Vibrational Levels of S_1 States. *Phys. Chem. Chem. Phys.* **2018**, *20*, 26859–26869.

(16) Tiwari, P.; Metternich, J. B.; Czar, M. F.; Zenobi, R. Breaking the Brightness Barrier: Design and Characterization of a Selected-Ion Fluorescence Measurement Setup with High Optical Detection Efficiency. *J. Am. Chem. Soc. Mass Spectrom.* **2020**, *32*, 187–197.

(17) Kjær, C.; Langeland, J.; Lindkvist, T. T.; Sørensen, E. R.; Stockett, M. H.; Kjaergaard, H. G.; Nielsen, S. B. A New Setup for Low-Temperature Gas-Phase Ion Fluorescence Spectroscopy. *Rev. Sci. Instrum.* **2021**, *92*, 033105.

(18) Frankevicha, V.; Guan, X.; Dashtiev, M.; Zenobi, R. Laser-Induced Fluoresence of Trapped Gas-Phase Molecular Ions Generated by Internal-Source Matrix-Assisted Laser Desorption/Ionization in a Fourier Transform Ion Cyclotron Resonance Mass Spectrometer. *Eur. J. Mass Spectrom.* **2005**, *11*, 475–482.

(19) Wu, R.; Metternich, J. B.; Tiwari, P.; Zenobi, R. Adapting a Fourier Transform Ion Cyclotron Resonance Mass Spectrometer for Gas-Phase Fluorescence Spectroscopy Measurement of Trapped Biomolecular Ions. *Anal. Chem.* **2021**, *93*, 15626–15632.

(20) Friedrich, J.; Fu, J.; Hendrickson, C. L.; Marshall, A. G.; Wang, Y.-S. Time Resolved Laser-Induced Fluorescence of Electrosprayed Ions Confined in a Linear Quadrupole Trap. *Rev. Sci. Instrum.* **2004**, *75*, 4511–4515.

(21) Rajagopal, V.; Stokes, C.; Ferzoco, A. A Linear Ion Trap with an Expanded Inscribed Diameter to Improve Optical Access for Fluorescence Spectroscopy. *J. Am. Soc. Mass Spectrom.* **2017**, *29*, 260–269.

(22) Nolting, D.; Malek, R.; Makarov, A. Ion Traps in Modern Mass Spectrometry. *Mass Spectrom. Rev.* **2017**, *38*, 150–168.

(23) Sagoo, S. K.; Jockusch, R. A. The Fluorescence Properties of Cationic Rhodamine B in the Gas Phase. *J. Photochem. Photobiol. A* **2011**, *220*, 173–178.

(24) Forbes, M. W.; Jockusch, R. A. Gas-Phase Fluorescence Excitation and Emission Spectroscopy of Three Xanthene Dyes (Rhodamine 575, Rhodamine 590 and Rhodamine 6G) in a Quadrupole Ion Trap Mass Spectrometer. *J. Am. Soc. Mass Spectrom.* **2011**, *22*, 93–109.

(25) Nagy, A. M.; Talbot, F. O.; Czar, M. F.; Jockusch, R. A. Fluorescence Lifetimes of Rhodamine Dyes *in Vacuo*. *J. Photochem. Photobiol. A* **2012**, *244*, 47–53.

(26) Kjær, C.; Lissau, H.; Gravesen Salinas, N. K.; Østergaard Madsen, A.; Stockett, M. H.; Storm, F. E.; Holm Hansen, T.; Andersen, J. U.; Laursen, B. W.; Mikkelsen, K. V. et al. Luminescence Spectroscopy of Rhodamine Homodimer Dications *in Vacuo* Reveals Strong Dye-Dye Interactions. *ChemPhysChem* **2019**, *20*, 533–537.

(27) Kung, J. C. K.; Forman, A.; Jockusch, R. A. The Effect of Methylation on the Intrinsic Photophysical Properties of Simple Rhodamines. *Phys. Chem. Chem. Phys.* **2019**, *21*, 10261–10271.

(28) Petersen, A. U.; Kjær, C.; Jensen, C.; Nielsen, M. B.; Nielsen, S. B. Gas-Phase Ion Fluorescence Spectroscopy of Tailor-Made Rhodamine Homo- and Heterodyads: Quenching of Electronic Communication by π-Conjugated Linkers. *Angew. Chem. Int. Ed.* **2020**, *59*, 20946–20955.

(29) McQueen, P. D.; Sagoo, S.; Yao, H.; Jockusch, R. A. On the Intrinsic Photophysics of Fluorescein. *Angew. Chem. Int. Ed.* **2010**, *49*, 9193–9196.

(30) Yao, H.; Jockusch, R. A. Fluorescence and Electronic Action Spectroscopy of Mass-Selected Gas-Phase Fluorescein, 2′,7′-Dichlorofluorescein, and 2′,7′-Difluorofluorescein Ions. *J. Phys. Chem. A* **2013**, *117*, 1351–1359.

(31) Kjær, C.; Hansson, R. F.; Hedberg, C.; Jensen, F.; Jensen, H. H.; Nielsen, S. B. Gas-Phase Action and Fluorescence Spectroscopy of Mass-Selected Fluorescein Monoanions and Two Derivatives. *Phys. Chem. Chem. Phys.* **2020**, *22*, 9210–9215.

(32) Stockett, M. H.; Kjær, C.; Daly, S.; Bieske, E. J.; Verlet, J. R. R.; Nielsen, S. B.; Bull, J. N. Photophysics of Isolated Rose Bengal Anions. *J. Phys. Chem. A* **2020**, *124*, 8429–8438.

(33) Vogt, E.; Langeland, J.; Kjær, C.; Lindkvist, T. T.; Kjaergaard, H. G.; Nielsen, S. B. Effect of Freezing out Vibrational Modes on Gas-Phase Fluorescence Spectra of Small Ionic Dyes. *J. Phys. Chem. Lett.* **2021**, *12*, 11346–11352.

(34) Djavani-Tabrizi, I.; Jockusch, R. A. Gas-Phase Fluorescence of Proflavine Reveals Two Close-Lying, Brightly Emitting States. *J. Phys. Chem. Lett.* **2022**, *13*, 2187–2192.

(35) Danell, A. S.; Parks, J. H. FRET Measurements of Trapped Oligonucleotide Duplexes. *Int. J. Mass Spectrom.* **2003**, *229*, 35–45.

(36) Czar, M. F.; Zosel, F.; König, I.; Nettels, D.; Wunderlich, B.; Schuler, B.; Zarrine-

Afsar, A.; Jockusch, R. A. Gas-Phase FRET Efficiency Measurements To Probe the Conformation of Mass-Selected Proteins. *Anal. Chem.* **2015**, *87*, 7559–7565.

(37) Clegg, R. M. *Fret and Flim Techniques*; Elsevier, 2009; pp 1–57.

(38) Kjær, C.; Langeland, J.; Nielsen, S. B. Intrinsic Fluorescence from Firefly Oxyluciferin Monoanions Isolated *in Vacuo*. *Phys. Chem. Chem. Phys.* **2022**, 18505–18510.

(39) O'Keefe, A.; Deacon, D. A. G. Cavity Ring-Down Optical Spectrometer for Absorption Measurements Using Pulsed Laser Sources. *Rev. Sci. Instrum.* **1988**, *59*, 2544–2551.

(40) Berden, G.; Peeters, R.; Meijer, G. Cavity Ring-Down Spectroscopy: Experimental Schemes and Applications. *Int. Rev. Phys. Chem.* **2000**, *19*, 565–607.

(41) Polfer, N. C.; Dugourd, P. *Laser Photodissociation and Spectroscopy of Mass-Separated Biomolecular Ions*; Springer London, Limited, 2013; p 119.

(42) Tureček, F. UV-Vis Spectroscopy of Gas-Phase Ions. *Mass Spectrom. Rev.* **2021**, 1–21.

(43) Gunzer, F.; Krüger, S.; Grotemeyer, J. Photoionization and Photofragmentation in Mass Spectrometry With Visible and UV Lasers. *Mass Spectrom. Rev.* **2018**, *38*, 202–217.

(44) Nielsen, S. B., Wyer, J. A., Eds. *Photophysics of Ionic Biochromophores*; Springer Berlin Heidelberg, 2013.

(45) Markworth, P. B.; Adamson, B. D.; Coughlan, N. J. A.; Goerigk, L.; Bieske, E. J. Photoisomerization Action Spectroscopy: Flicking the Protonated Merocyanine–Spiropyran Switch in the Gas Phase. *Phys. Chem. Chem. Phys.* **2015**, *17*, 25676–25688.

(46) Baercor, T.; Mayerfn, P. M. Statistical Rice-Ramsperger-Kassel-Marcus Quasiequilibrium Theory Calculations in Mass Spectrometry. *J. Am. Soc. Mass Spectrom.* **1997**, *8*, 103–115.

(47) Støchkel, K.; Milne, B. F.; Nielsen, S. B. Absorption Spectrum of the Firefly Luciferin Anion Isolated *in Vacuo*. *J. Phys. Chem. A* **2011**, *115*, 2155–2159.

(48) Bull, J. N.; Scholz, M. S.; Carrascosa, E.; da Silva, G.; Bieske, E. J. Double Molecular Photoswitch Driven by Light and Collisions. *Phys. Rev. Lett.* **2018**, *120*, 223002.

(49) Oberheide, J.; Wilhelms, P.; Zimmer, M. New Results on the Absolute Ion Detection Efficiencies of a Microchannel Plate. *Meas. Sci. Technol.* **1997**, *8*, 351–354.

(50) Kubin, R.; Fletcher, A. Fluorescence Quantum Yields of Some Rhodamine Dyes. *J. Luminesc.* **1982**, *27*, 455–462.

(51) Magde, D.; Wong, R.; Seybold, P. G. Fluorescence Quantum Yields and Their Relation to Lifetimes of Rhodamine 6G and Fluorescein in Nine Solvents: Improved Absolute Standards for Quantum Yields. *Photochem. Photobiol.* **2007**, *75*, 327–334.

(52) Martin, M. M. Hydrogen Bond Effects on Radiationless Electronic Transitions in Xanthene Dyes. *Chem. Phys. Lett.* **1975**, *35*, 105–111.

(53) Zhou, P.; Tang, Z.; Li, P.; Liu, J. Unraveling the Mechanism for Tuning the Fluorescence of Fluorescein Derivatives: The Role of the Conical Intersection and $n\pi^*$ State. *J. Phys. Chem. Lett.* **2021**, *12*, 6478–6485.

(54) Horke, D. A.; Chatterley, A. S.; Bull, J. N.; Verlet, J. R. R. Time-Resolved Photodetachment Anisotropy: Gas-Phase Rotational and Vibrational Dynamics of the Fluorescein Anion. *J. Phys. Chem. Lett.* **2014**, *6*, 189–194.

(55) Jares-Erijman, E. A.; Jovin, T. M. FRET Imaging. *Nat. Biotech.* **2003**, *21*, 1387–1395.

(56) Miura, T.; Urano, Y.; Tanaka, K.; Nagano, T.; Ohkubo, K.; Fukuzumi, S. Rational Design Principle for Modulating Fluorescence Properties of Fluorescein-Based Probes by Photoinduced Electron Transfer. *J. Am. Chem. Soc.* **2003**, *125*, 8666–8671.

(57) Urano, Y.; Kamiya, M.; Kanda, K.; Ueno, T.; Hirose, K.; Nagano, T. Evolution of Fluorescein as a Platform for Finely Tunable Fluorescence Probes. *J. Am. Chem. Soc.* **2005**, *127*, 4888–4894.

(58) Lavis, L. D. Teaching Old Dyes New Tricks: Biological Probes Built from Fluoresceins and Rhodamines. *Ann. Rev. Biochem.* **2017**, *86*, 825–843.

(59) Turnbull, J. L.; Benlian, B. R.; Golden, R. P.; Miller, E. W. Phosphonofluoresceins: Synthesis, Spectroscopy, and Applications. *J. Am. Chem. Soc.* **2021**, *143*, 6194–6201.

(60) Rajasekar, M. Recent Development in Fluorescein Derivatives. *J. Mol. Struct.* **2021**, *1224*, 129085.

(61) Zheng, H.; Zhan, X.-Q.; Bian, Q.-N.; Zhang, X.-J. Advances in Modifying Fluorescein and Rhodamine Fluorophores as Fluorescent Chemosensors. *Chem. Commun.* **2013**, *49*, 429–447.

(62) Crovetto, L.; Paredes, J. M.; Rios, R.; Talavera, E. M.; Alvarez-Pez, J. M. Photophysics of a Xanthenic Derivative Dye Useful as an "On/Off" Fluorescence Probe. *J. Phys. Chem. A* **2007**, *111*, 13311–13320.

(63) Kjær, C.; Nielsen, S. B.; Stockett, M. H. Sibling Rivalry: Intrinsic Luminescence from Two Xanthene Dye Monoanions, Resorufin and Fluorescein, Provides Evidence for Excited-State Proton Transfer in the Latter. *Phys. Chem. Chem. Phys.* **2017**, *19*, 24440–24444.

(64) Horke, D. A.; Chatterley, A. S.; Verlet, J. R. R. Effect of Internal Energy on the Repulsive Coulomb Barrier of Polyanions. *Phys. Rev. Lett.* **2012**, *108*, 083003.

(65) Yao, H.; Steill, J. D.; Oomens, J.; Jockusch, R. A. Infrared Multiple Photon Dissociation Action Spectroscopy and Computational Studies of Mass-Selected Gas-Phase Fluorescein and 2′,7′-Dichlorofluorescein Ions. *J. Phys. Chem. A* **2011**, *115*, 9739–9747.

(66) Tanabe, T.; Saito, M.; Noda, K.; Starikov, E. B. Molecular Structure Conversion of Fluorescein Monoanions in an Electrostatic Storage Ring. *Eur. Phys. J. D* **2012**, *66*, 163.

(67) Gronert, S. Estimation of Effective Ion Temperatures in a Quadrupole Ion Trap. *J. Am. Chem. Mass Spectrom.* **1998**, *9*, 845–848.

(68) Aßmann, J.; Kling, M.; Abel, B. Watching Photoinduced Chemistry and Molecular Energy Flow in Solution in Real Time. *Angew. Chem. Int. Ed.* **2003**, *42*, 2226–2246.

(69) Birks, J. B.; Dyson, D. J. The Relations Between the Fluorescence and Absorption Properties of Organic Molecules. *Proc. Royal Soc. Lon. A.* **1963**, *275*, 135–148.

(70) Svendsen, A.; Kiefer, H. V.; Pedersen, H. B.; Bochenkova, A. V.; Andersen, L. H. Origin of the Intrinsic Fluorescence of the Green Fluorescent Protein. *J. Am. Chem. Soc.* **2017**, *139*, 8766–8771.

(71) Gruber, E.; Kabylda, A. M.; Nielsen, M. B.; Rasmussen, A. P.; Teiwes, R.; Kusochek, P. A.; Bochenkova, A. V.; Andersen, L. H. Light Driven Ultrafast Bioinspired Molecular Motors: Steering and Accelerating Photoisomerization Dynamics of Retinal. *J. Am. Chem. Soc.* **2021**, *144*, 69–73.

(72) van Leeuwen, T.; Lubbe, A. S.; Štacko, P.; Wezenberg, S. J.; Feringa, B. L. Dynamic Control of Function by Light-Driven Molecular Motors. *Nat. Rev. Chem.* **2017**, *1*, 0096.

(73) Goulet-Hanssens, A.; Eisenreich, F.; Hecht, S. Enlightening Materials with Photoswitches. *Adv. Mat.* **2020**, *32*, 1905966.

(74) Klonis, N.; Sawyer, W. H. Spectral Properties of the Prototropic Forms of Fluorescein in Aqueous Solution. *J. Fluorescence* **1996**, *6*, 147–157.

(75) Wolk, A. B.; Leavitt, C. M.; Garand, E.; Johnson, M. A. Cryogenic Ion Chemistry and Spectroscopy. *Acc. Chem. Res.* **2013**, *47*, 202–210.

(76) March, R. E. Quadrupole Ion Traps. *Mass Spectrom. Rev.* **2009**, *28*, 961–989.

(77) Frankevich, V.; Sinues, P. M.-L.; Barylyuk, K.; Zenobi, R. Ion Mobility Spectrometry Coupled to Laser-Induced Fluorescence. *Anal. Chem.* **2013**, *85*, 39–43.

(78) Frankevich, V. E.; Barylyuk, K. V.; Sinues, P. M.-L.; Zenobi, R. Ion Mobility Spectrometry Coupled to Laser-Induced Fluorescence For Probing the Electronic Structure and Conformation of Gas-Phase Ions. *J. Anal. Chem.* **2014**, *69*, 1215–1219.

(79) Eiceman, G. A.; Karpas, Z.; Hill, H. H. *Ion Mobility Spectrometry*; Taylor & Francis Group, 2016; p 444.

(80) Bull, J. N.; Carrascosa, E.; Mallo, N.; Scholz, M. S.; da Silva, G.; Beves, J. E.; Bieske, E. J. Photoswitching an Isolated Donor–Acceptor Stenhouse Adduct. *J. Phys. Chem. Lett.* **2018**, *9*, 665–671.

(81) Bull, J. N.; Coughlan, N. J. A.; Bieske, E. J. Protomer-Specific Photochemistry Investigated Using Ion Mobility Mass Spectrometry. *J. Phys. Chem. A* **2017**, *121*, 6021–6027.

(82) Bull, J. N.; da Silva, G.; Scholz, M. S.; Carrascosa, E.; Bieske, E. J. Photoinitiated Intramolecular Proton Transfer in Deprotonated *para*-Coumaric Acid. *J. Phys. Chem. A* **2019**, *123*, 4419–4430.

(83) Lanucara, F.; Holman, S. W.; Gray, C. J.; Eyers, C. E. The Power of Ion Mobility-Mass Spectrometry for Structural Characterization and the Study of Conformational Dynamics. *Nat. Chem.* **2014**, *6*, 281–294.

(84) Haas, E. The Study of Protein Folding and Dynamics by Determination of Intramolecular Distance Distributions and Their Fluctuations Using Ensemble and Single-Molecule FRET Measurements. *ChemPhysChem* **2005**, *6*, 858–870.

(85) Schuler, B.; Eaton, W. A. Protein Folding Studied by Single-Molecule FRET. *Cur. Op. Struct. Biol.* **2008**, *18*, 16–26.

(86) Jarrold, M. F. Peptides and Proteins in the Vapor Phase. *Annu. Rev. Phys. Chem.* **2000**, *51*, 179–207.

(87) de Vries, M. S.; Hobza, P. Gas-Phase Spectroscopy of Biomolecular Building Blocks. *Annu. Rev. Phys. Chem.* **2007**, *58*, 585–612.

(88) Zhou, S.; Cook, K. D. Probing Solvent Fractionation in Electrospray Droplets with Laser-Induced Fluorescence of a Solvatochromic Dye. *Anal. Chem.* **2000**, *72*, 963–969.

(89) Rodriguez-Cruz, S. E.; Khoury, J. T.; Parks, J. H. Protein Fluorescence Measurements Within Electrospray Droplets. *J. Am. Soc. Mass Spectrom.* **2001**, *12*, 716–725.

(90) Szarka, M.; Szigeti, M.; Guttman, A. Imaging Laser-Induced Fluorescence Detection at the Taylor Cone of Electrospray Ionization Mass Spectrometry. *Anal. Chem.* **2019**, *91*, 7738–7743.

(91) Tiwari, P.; Czar, M. F.; Zenobi, R. Fluorescence-Based Detection of the Desolvation Process of Protein Ions Generated in an Aqueous Electrospray Plume. *Anal. Chem.* **2021**, *93*, 3635–3642.

TOC Graphic